The analysis of dielectric relaxation phenomena with the inverse Fourier transformation

Karel Liedermann, Alois Loidl

Angaben zur Veröffentlichung / Publication details:

Liedermann, Karel, and Alois Loidl. 1993. "The analysis of dielectric relaxation phenomena with the inverse Fourier transformation." *Journal of Non-Crystalline Solids* 155 (1): 26–36. https://doi.org/10.1016/0022-3093(93)90468-d.

The analysis of dielectric relaxation phenomena with the inverse Fourier transformation

Karel Liedermann and Alois Loidl [1]

Institut für Physik, Johannes-Gutenberg-Universität, W-6500 Mainz 1, Germany

A method to determine the distribution of relaxation times directly from dielectric loss spectra is presented. The method is based upon a deconvolution procedure: the Fourier transform of the loss factor is divided by $\mathrm{sech}(\pi^2 f)$ and then, via an inverse Fourier transformation, transformed into the time domain. Limitations and possible improvements of the method are discussed. It is shown that the present method is able to reveal local relaxation processes not perceptible in the loss factor spectrum. With simulated noise-free data, the resolution of the method is one third of a decade on a logarithmic relaxation timescale.

1. Introduction

Dielectric spectra in complex systems reveal broad and sometimes asymmetric dispersion steps and loss peaks. The analysis is usually carried out in terms of phenomenological expressions (Cole–Cole, Cole–Davidson, Havriliak–Negami) or assuming a distribution of hindering barriers (Gauss, Fröhlich). Asymmetric spectra are often modelled using the imaginary Laplace transform of the Kohlrausch–Williams–Watts (KWW) function which describes a stretched exponential decay of the polarization in the time domain. In the latter case, an intrinsically non-exponential relaxation behaviour is often assumed and described in terms of serial processes (e.g., time-dependent relaxation rates [1], universal dielectric response [2] or hierarchically constrained relaxations [3]). However, in most cases, a distribution of relaxation times resulting from parallel processes in a spatially heterogeneous medium cannot be excluded. The relaxation of each relaxing particle is then usually assumed to be exponential (leading to the Debye-shape peaks in the frequency domain) and the experimentally observed departures from the Debye behaviour are interpreted as a consequence of the presence of many parallel mechanisms with differing timescales [4]. The dispute concerning the interpretation of these relaxation spectra is thus far from being settled and experimental proofs of the character of the relaxation mechanism are rather rare [5].

In the following, a method for the direct calculation of the distribution of relaxation times is presented. Assuming parallel processes, the experimental data are directly converted into a distribution of relaxation times without any underlying phenomenological model. It is necessary to emphasize that the model can only be used in systems with heterogeneous distribution of exponential relaxation times: for example, systems with quenched disorder leading to a distribution of hindering barriers or to random fields and composite materials.

The interpretation of dielectric spectra in terms of distribution of relaxation times becomes even

[1] Present address: Institut für Festkörperphysik, TH Darmstadt, 6100 Darmstadt, Germany.

Correspondence to: Dr K. Liedermann, Department of Physics, Faculty of Electrical Engineering, Technical University, 602 00 Brno, Czechoslovakia (permanent address).

more important in the analysis of systems with different relaxation processes. Such problems arise, for example, in systems with α- and β-relaxations which can hardly be separated near the glass transition temperature, yielding an asymmetric primary relaxation. The details of the temperature dependence of relaxation rates of α- and β-processes in the crossover region are debated. It is still an open question whether α- and β-relaxation rates merge [6] or cross [7] near the glass transition temperature.

Careful analysis of individual relaxation mechanisms is particularly demanded in composite dielectric materials with individual components which have different relaxation channels. Due to overlapping, the resulting loss factor shows only poorly resolved peaks or shoulders, thus rendering the resolution of relaxations difficult.

Assuming a distribution of relaxation times, $g(\tau)$, the complex permittivity is expressed as

$$\hat{\epsilon}(\omega) = \epsilon_\infty + (\epsilon_s - \epsilon_\infty)\int_0^\infty \frac{g(\tau)}{1 + j\omega\tau}\, d\tau, \qquad (1)$$

where $\hat{\epsilon}$ is the complex permittivity, ϵ_∞, ϵ_s are the optical and static permittivities, respectively, ω is the angular frequency and j is the imaginary unit. Function $g(\tau)$ is the probability density of the distribution of relaxation times satisfying the condition

$$\int_0^\infty g(\tau)\, d\tau = 1. \qquad (2)$$

The loss factor is the imaginary part of the complex permittivity

$$\epsilon''(\omega) = (\epsilon_s - \epsilon_\infty)\int_0^\infty \frac{g(\tau)\omega\tau}{1 + \omega^2\tau^2}\, d\tau. \qquad (3)$$

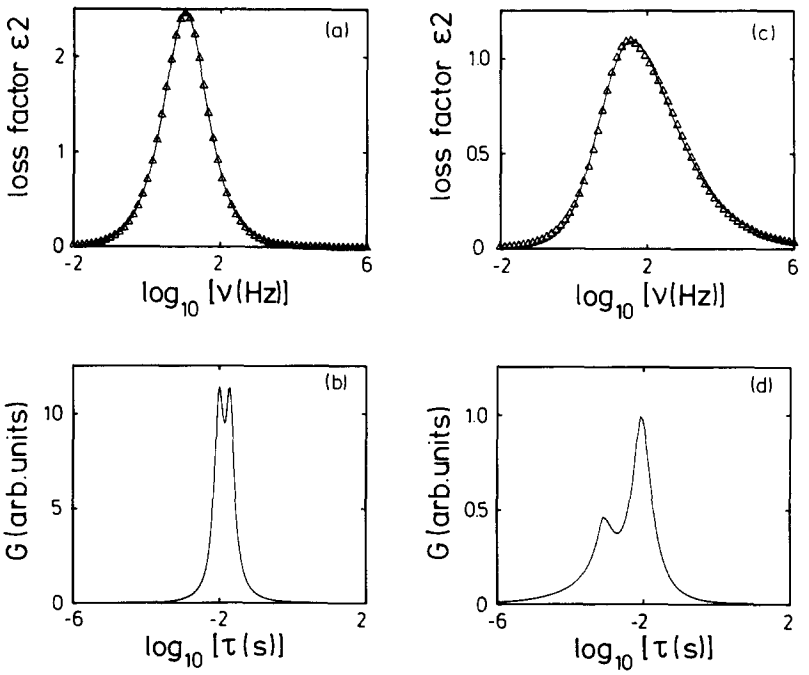

Fig. 1. (a) Loss factor vs. frequency generated from two Cole–Cole distributions with $\alpha_1 = \alpha_2 = 0.1$, $\tau_1 = 0.01$ s, $\tau_2 = 0.02$ s and equal weights (△) and fit with one Cole–Cole distribution (———). (b) Source distribution, $G(u)$, for loss factor in (a). (c) Loss factor vs. frequency generated out of two Havriliak–Negami distributions with $\alpha_1 = 0.2$, $\gamma_1 = 0.7$, $\tau_1 = 0.01$ s, $\Delta\epsilon_1 = 3$, $\alpha_2 = 0.2$, $\gamma_2 = 0.8$, $\tau_2 = 0.001$ s, $\Delta\epsilon_2 = 1.5$ (△) and fit with a single KWW function (———). (d) Source distribution for (c).

Since in many materials the observed loss peaks and hence distributions of relaxation times are rather broad, covering several decades of frequency, eq. (3) is preferably written in the form

$$\epsilon''(\omega) = (\epsilon_s - \epsilon_\infty)\int_{-\infty}^{+\infty} \frac{\omega\tau G(\ln\tau)\, \mathrm{d}(\ln\tau)}{1+\omega^2\tau^2}, \quad (4)$$

where

$$G(\ln\tau) = \tau g(\tau). \quad (5)$$

Two simulated loss factor curves are shown in fig. 1(a) and fig. 1(c) (△). Such curves are usually analyzed using phenomenological expressions as

$$\hat{\epsilon}(\omega) = \epsilon_\infty + \frac{\epsilon_s - \epsilon_\infty}{\left[1-(j\omega\tau)^{1-\alpha}\right]^\beta}, \quad (6)$$

$\alpha = 0, \beta = 1$ Debye,

$0 < \alpha < 1, \beta = 1$ Cole–Cole,

$\alpha = 0, 0 < \beta < 1$ Cole–Davidson,

$0 < \alpha < 1, 0 < \beta < 1$ Havriliak–Negami

or

$$\hat{\epsilon}(\omega) = F\left\{\exp\left[-(t/\tau)^\beta\right]\right\}, \quad 0 < \beta < 1, \quad (7)$$

where F indicates one-sided Fourier transform (FT) from time to frequency domain. Equation (7) is known as the Kohlrausch–Williams–Watts (KWW) function.

The dielectric loss spectra shown in fig. 1(a) and fig. 1(c) were created from $G(\ln\tau)$ as given in fig. 1(b) and fig. 1(d), respectively, i.e., in both cases two relaxation mechanisms were assumed. The loss spectra in fig. 1(a) and fig. 1(c) were fitted with formulas (6) and (7), i.e., with a single relaxation mechanism. The fits (solid lines) are quite good; however, by virtue of the two underlying relaxation mechanisms present in $G(\ln\tau)$, they are misleading. Figure 1 proves the well-known fact that, if the individual relaxation mechanisms are on the timescale too close to each other, then after transformation (3) they are no more separable in the frequency domain and reveal a single broader peak in $\epsilon''(\omega)$.

The separation of relaxation mechanisms will become worse in a practical case where conductivity contributions and experimental noise are inevitable. The analysis of relaxation mechanisms therefore requires a solution of eq. (4) with experimental data, i.e., in the presence of noise.

Several methods to calculate $G(\ln\tau)$ from the $\epsilon''(\omega)$ are available. If the expression for $\hat{\epsilon}(\omega)$ is known in closed form, it is possible to calculate $G(\ln\tau)$ from the singularities of $\hat{\epsilon}(\omega)$ in the upper half of the complex plane [4]:

$$G(\ln\tau) = \frac{1}{2\pi(\epsilon_s - \epsilon_\infty)} \lim_{\omega\to 0}\left\{\mathrm{Im}\left[\hat{\epsilon}\left(-\omega + \frac{j}{\tau}\right)\right] - \mathrm{Im}\left[\hat{\epsilon}\left(+\omega + \frac{j}{t}\right)\right]\right\}. \quad (8)$$

However, for most cases $\hat{\epsilon}(\omega)$ is known only in isolated points and eq. (8) is not applicable.

For numerical methods, the early literature is surveyed in refs. [4] and [8]. Other methods are suggested in refs. [9–12].

2. Theory

The solution of the problem presented here is based upon the Fourier transformation of eq. (4) and the deconvolution of $G(\ln\tau)$. This method has been already applied by Franklin and de Bruin [12] and Misell and Sheppard [13] for dielectric data. A review of this method for general use is given in ref. [14]. However, deconvolution method is more often discussed than actually used [15]. The results are still not very satisfactory. The authors in ref. [12] do not explicitly state the resolution of their method, but in an example they resolve two relaxation mechanisms which are separated one decade in frequency. The method presented below aims at resolving the relaxation peaks only a factor of two apart with simulated noise-free data.

First, eq. (4) is modified in such a way that it is suitable for the Fourier transformation. After introducing a substitution

$$x = \ln\omega/\omega_0, \quad y = \ln\omega\tau, \quad (9)$$

where

$$\omega_0 = \sqrt{\omega_1\omega_2}, \quad (10)$$

where ω_1 and ω_2 are the boundaries of the experimentally accessible frequency window, eq. (4) can be written as

$$\epsilon''(x) = \int_{-\infty}^{+\infty} g\left(\frac{1}{\omega_0}\exp(y-x)\right) \times \frac{1}{\omega_0}\exp(y-x)\frac{\exp(y)}{1+\exp(2y)}\,dy, \tag{11}$$

where

$$\tau = \frac{1}{\omega_0}\exp(y-x), \tag{12}$$

$$dy = d(\ln\tau\omega_0) = d(\ln\tau). \tag{13}$$

Considering eq. (5), eq. (11) may be rewritten in the form

$$\epsilon''(x) = \tfrac{1}{2}\int_{-\infty}^{+\infty} G(y-x)\,\mathrm{sech}y\,dy. \tag{14}$$

The integral in eq. (14) is a well-known correlation integral whose Fourier transformation yields

$$F\{\epsilon''(x)\} = F^*\{G(u)\}F\{\mathrm{sech}y\} \tag{15}$$

or, if separate symbols are introduced to denote Fourier transforms,

$$E(f) = Q^*(f)S(f). \tag{16}$$

An asterisk in eqs. (15) and (16) denotes a complex conjugate value. After some rearrangements, an expression for $G(u) = G(\ln\tau)$ is obtained as

$$G(u) = F^{-1}\left\{\left[\frac{F\{\epsilon''(x)\}}{F\{\mathrm{sech}x\}}\right]^*\right\}, \tag{17}$$

$$G(u) = F^{-1}\left\{\left[\frac{E(f)}{S(f)}\right]^*\right\}. \tag{18}$$

If $\epsilon''(x)$ is known in closed form, then eq. (18) yields directly the expression for $G(u)$ as in eq. (8), provided the Fourier transforms are available in closed form as well. With experimental data, the expression for $\epsilon''(x)$ is never known analytically and therefore the operations indicated in eq. (18) have to be performed numerically.

The authors in ref. [12] based their procedure on utilizing the properties of the circular convolution. The circular (periodical) convolution of two functions is equal to its non-periodical counterpart only if both functions are defined in one half of the total interval, on which $\epsilon''(x)$ is defined, and are zero elsewhere [16]. Therefore in ref. [12] it is suggested to perform the discrete Fourier transformation (DFT) of $\epsilon''(x)$ in the experimentally available frequency window, the DFT of *sech*y on an interval of the half length of the frequency window, then to perform the division and to remove 'Fourier noise' appearing after the division by truncating the result at a suitable point. The selection of the truncation interval in such a case is quite difficult, regarding the fact that the 'Fourier noise' may contain valuable information about the structure of $G(\ln\tau)$ which is then lost. In the procedure described here, the idea of the circular convolution was abandoned and an attempt was made to approximate the analytical expression for the FT of $\epsilon''(x)$ (on an infinite interval) by the DFT in the given frequency window. Next, formulas for DFT are given and then deviations from the analytical FT are discussed.

In view of the fact that the fast Fourier transformation (FFT) algorithm is used, it is desirable, although not necessary, that the number of input datapoints be $N = 2^m$. The datapoints are assumed to be available at frequencies, ω_i, satisfying the relation

$$\omega_{i+1} = \omega_i \exp T, \quad i = 1, 2, \ldots, N-1, \tag{19}$$

i.e., they are located at equidistant intervals on a logarithmic scale. Frequencies ω_i are transformed according to eq. (9); the value of ω_0 (eq. (10)) is set by the condition that the transformed values x_i are located symmetrically at both sides of the origin:

$$x_1 = x_{\min} = -x_N = -x_{\max}, \tag{20}$$

$$x_i = \left(i - 1 - \frac{N-1}{2}\right)T, \quad i = 1, 2, \ldots, N, \tag{21}$$

$$T = \frac{\ln\omega_N/\omega_1}{N-1}. \tag{22}$$

The Fourier transformation is now performed on a single-sided, non-symmetrical interval

$\langle 0,1/T\rangle$ and the equation for the DFT can be written as

$$E\left(\frac{i}{NT}\right) = \sum_{k=0}^{N-1} \epsilon''\left(\left(k-\frac{N-1}{2}\right)T\right) \times \exp\left[-2\pi ji\left(k-\frac{N-1}{2}\right)/N\right],$$

$$i = 0, 1, \ldots, N-1. \qquad (23)$$

After some rearrangements, eq. (23) is obtained in a slightly modified form:

$$E\left(\frac{i}{NT}\right) = \exp\left(\frac{2\pi ji}{N}\frac{N-1}{2}\right) \times \sum_{k=0}^{N-1} \epsilon''\left(\left(k-\frac{N-1}{2}\right)T\right) \times \exp(-2\pi ijk/N),$$

$$i = 0, 1, \ldots, N-1. \qquad (24)$$

The sum may be evaluated by the FFT [16]. The inversion of eq. (23) is similarly obtained by changing the sign in the exponential term in eq. (23), thus yielding

$$G\left(\left(k-\frac{N-1}{2}\right)T\right) = \sum_{i=0}^{N-1} Q^*\left(\frac{i}{NT}\right) \exp\left[2\pi ji\left(k-\frac{N-1}{2}\right)/N\right],$$

$$k = 0, 1, \ldots, N-1. \qquad (25)$$

Separating the exponential term into two parts and introducing $P(i)$,

$$P(i) = Q^*\left(\frac{i}{NT}\right) \exp\left(-\frac{2\pi ji}{N}\frac{N-1}{2}\right), \qquad (26)$$

converts eq. (25) to a standard FFT formula:

$$G\left(\left(k-\frac{N-1}{2}\right)T\right) = \sum_{i=0}^{N-1} P(i) \exp(2\pi jik/N),$$

$$k = 0, 1, \ldots, N-1. \qquad (27)$$

In view of the properties of the DFT, only the first half of $E(i/NT)$ values are independent (up to $= N/2$), the rest being the symmetrical continuation of the first half. Thus the highest available frequency component is at

$$f_{max} = 1/2T. \qquad (28)$$

The fundamental problem in calculating the FT in eq. (18) is to what extent the numerical FTs in eqs. (23) and (25) agree with their analytical counterparts? The analytical expression of the FT of a given function agrees exactly with its DFT only under very special conditions (periodicity of the function, sampling interval equal to an integer multiple of the period, rate of sampling twice as high as maximum frequency component present), which are seldom met in practice, certainly not for dielectric data. Therefore the DFT of $\epsilon''(x)$ seriously departs from its theoretical value.

There are four main sources of deviations of the DFT from the analytical FT – truncation effects (i), aliasing (ii), computing errors (iii) and noise in the input data (iv). Since these effects sum up particularly in the vicinity of $i = N/2$ ($f = 1/2T$), the values of $E(f)$ (eq. (23)) for large i are dominated by noise, even for perfect, i.e., noise-free, data. Therefore, the values of $E(f)$ do not decay towards zero but rather remain constant. Consequently, $F\{G(u)\}$ does not decay towards zero either but oscillates with a large amplitude for large i. To obtain the 'true' behaviour of $G(u)$ it is necessary to assume that the frequency components for $i > i_{max}$ do not contain any useful physical information and to set them equal to zero. However, since the high frequency components contain a valuable information about the fine details of $G(u)$, it is desirable to extend the range of 'true' frequency components as far as possible, in other words to set i_{max} as close as possible to $N/2$. Procedures for achieving this are further examined in more detail.

(i) The truncation effect is due to a finite interval length, so that the definition integral of the FT,

$$F\{x(t)\} = \int_{-\infty}^{+\infty} x(t) \exp(-2\pi jft)\, dt, \qquad (29)$$

is substituted by

$$F\{x(t)\} = \int_{-T_0/2}^{+T_0/2} x(t) \exp(-2\pi jft)\, dt. \qquad (30)$$

In order to suppress truncation effects, the measured data were extrapolated to such values that corresponded to the precision of data processing

in the computer. For double-precision arithmetics, the extrapolation was performed until the extrapolated values decreased to values $< 10^{-12}$ in some cases and $< 10^{-14}$ in others. The idea behind the extrapolation was to find the FT of the full loss factor curve and not just the truncated FT of the loss factor in the experimentally available frequency window.

The extrapolation was mostly of the form

$$\epsilon''(f) = Af^m, \tag{31}$$

where A and m were chosen in such a way that the extrapolation matched the measured data in the value and in the first differential. In some cases, particularly with broad asymmetric loss peaks in polymers, this extrapolation leads to a very slow decrease and consequently to unphysically low or high frequencies. In these cases other extrapolations were used.

In order to investigate the influence of different extrapolations on the shape of the resulting $G(u)$, three more extrapolation formulas were tested:

$$\epsilon''(f) = A(\ln f - m)^{\alpha}, \tag{32}$$

$$e''(f) = A \exp\left[-\beta\sqrt{|\ln f - m|}\right], \tag{33}$$

$$e''(f) = A \exp\left[-\gamma(\ln f - m)^2\right], \tag{34}$$

which yield both slower and faster decrease on both sides of the loss spectrum. Parameters A and m were chosen so that the extrapolation matched the value and the first differential of the loss factor; parameters α, β and γ were varied to model differing steepness of the extrapolation.

If the extrapolation decreases slowly, then $G(u)$ decreases accordingly slowly as well. However, if the decrease of the extrapolated spectrum is too slow (in eq. (33) $\beta < 0.5$), the resulting distribution does not decrease to zero, but to some positive value. If the decrease of the extrapolated spectrum is fast, then the FT of $\epsilon''(x)$ contains too many high-amplitude high-frequency components. When only few of them are considered for the inverse FT, the resulting distribution $G(u)$ is smooth but the fine details including possible local peaks are smoothed out. When too many high-frequency components are considered for the inverse FT – in other words if the truncation point, $i_{\max} \to N/2$ – the resulting distribution, $G(u)$, exhibits a ripple which may screen small-amplitude local peaks. If the decrease of the extrapolated loss spectrum is too steep (in eq. (34) $\gamma > 0.1$), this decrease acts similarly as the truncation of the spectrum leading to a very slow decrease of $F\{\epsilon''(x)\}$. The truncation effects dominate the ratio, E/S, at relatively low values of i and thus only a few points may be used for the inverse FT. These few points for the inverse FT are not enough to recover the distribution and the resulting $G(u)$ contains spurious peaks and negative values.

In summary, if the conditions $\beta < 0.5$, $\gamma > 0.1$ are fulfilled, i.e., if the extrapolation is not an unphysical continuation of $\epsilon''(x)$, neither too steep nor too gradual, the resulting distribution, $G(u)$, shows no significant differences related to the extrapolation procedure used.

The influence of various factors on the FT may be estimated by plotting the power spectral density (PSD), $\Phi(f)$, defined as

$$\Phi(f) = |F\{\epsilon''(x)\}|^2. \tag{35}$$

The influence of the extrapolation on the truncation effects is clearly visible in fig. 2(a) for simulated data and in fig. 2(b) for experimental data.

For the unsymmetrical loss curve, the extrapolation resulted in different values of extrapolated loss factor at the end of the interval. This difference is known to lead to marked truncation effects [17]. Hence the extrapolated loss factor curve was shifted in such a way that the end values (i.e., $\epsilon''(f_{\min})$ and $\epsilon''(f_{\max})$) were as close to each other as possible.

The availability of the full loss factor curve and not just of its frequency window picture made it possible to consider the full FT of $\operatorname{sech} x$ on an infinite interval and not just its truncated DFT. The analytical form of $F\{\operatorname{sech} x\}$ is known [18] and is

$$F\{\operatorname{sech} x\} = \pi \operatorname{sech} \pi^2 f, \tag{36}$$

$$S\left(\frac{i}{NT}\right) = \pi \operatorname{sech}\left[\pi^2\left(\frac{i}{NT}\right)\right],$$

$$i = 0, 1, \ldots, N-1. \tag{37}$$

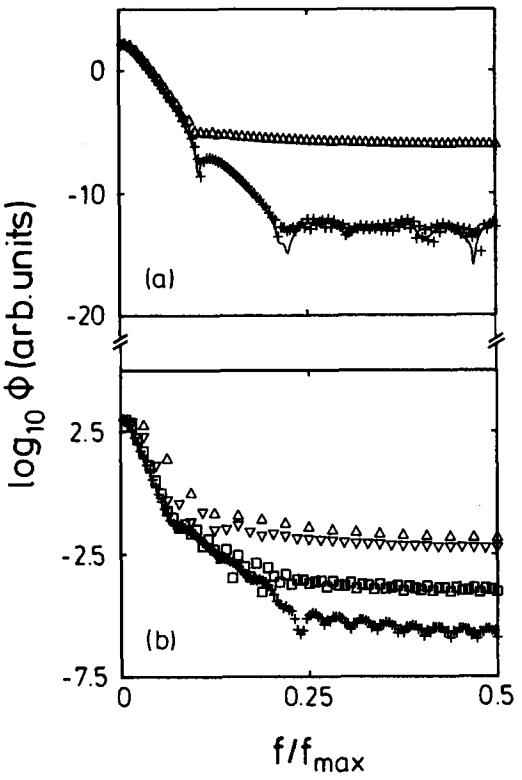

Fig. 2. Power spectra density vs. relative frequency. (a) For $\epsilon''(\omega)$ from fig. 1(a) without any extrapolation (△), with a single extrapolation (+) and with double extrapolation (———). (b) For $\epsilon''(\omega)$ on a sample of poly-ter-butylmethacrylate without any extrapolation (△), with a single extrapolation (▽), double extrapolation (□) and triple extrapolation (+).

The extrapolation procedure effectively removed truncation effects. However, one has to keep in mind that the obtained solution corresponds to the extrapolated loss factor. Thus, if the frequency window is too narrow or if a considerable portion of the relaxation lies outside the window, false results are due to occur.

(ii) Aliasing is due to setting [19]

$$\int_{kT}^{(k+1)T} x(t)\,\exp(-2\pi jft)\,\mathrm{d}t = x(kT)\,\exp(-2\pi jft)T \qquad (38)$$

in the DFT. Aliasing suppression was attempted by the use of several suitable window functions [14,16,20]. The results were varied; for example, Hanning and Kaiser windows were found to yield up to ten more points in the FT which could be used for the inverse FT, but in cases where the input loss factor was highly unsymmetrical, the use of windows led to a considerable distortion of the input loss factor curve and was therefore left out.

In addition, a polynomial interpolation [21] was used to correct aliasing as well. This polynomial interpolation (step-wise changes in eq. (38) are substituted by polynomials) brings the DFT closer to the analytical shape and in practical cases it turned out that it yields a few more datapoints for the inverse FT.

(iii) The third source of deviations are computation errors due to the finite precision of the data storage and processing in a computer. With the double-precision arithmetics, the difference between the maximum value of the PSD of $F\{\epsilon''(x)\}$ and the background is some 14–15 orders of magnitude (fig. 2), which suggests that using higher-precision arithmetics would probably further improve the results with simulated data.

(iv) The most serious source of errors is noise in the input data. Methods to suppress noise do exist [14], but they are based on implicit assumptions that the noise may be clearly separated in the power spectral density from the true signal. Under this assumption, the noise power spectral density may be described by a suitable simple empirical formula (straight line, exponential) and then subtracted from the total signal. If the power spectral density of the noise-free signal is $S(f)$ and that of the noise $N(f)$, the corrected FT is given by the formula [14]

$$E_{\mathrm{cor}}(f) = E(f)\,\frac{S(f)}{S(f)+N(f)}. \qquad (39)$$

To illustrate the influence of noise on the FT a random noise of the form $pr\epsilon''(x)$, where p varied between 10^{-1} and 10^{-6} and r was a random number between 0 and 1, was added to the loss factor prior to the FT. Examples of influence of the noise (where noise level is expressed in values of p) on the shape of $\Phi(f)$ are shown in fig. 3. The loss data were generated using two Cole–Cole distributions with $\tau_1 = 0.01$ s, $\tau_2 = 0.02$ s, $\alpha_1 = \alpha_2 = 0.1$ and equal strengths. The noise may

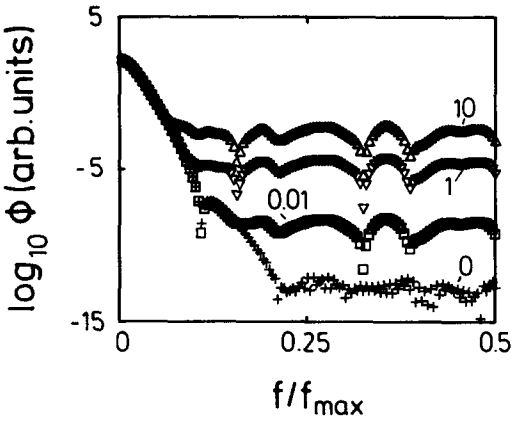

Fig. 3. Power spectral density vs. relative frequency for loss factor in fig. 1(a). Numbers indicate the level of noise expressed as p (see text).

be identified but it cannot be so easily described by a simple mathematical formula. Fitting this noise dominated region by a straight line and following application of eq. (39) did not lead to any dramatic improvement of the FT.

When inverting the ratio E/S, it turns out that the two relaxation maxima present in $G(u)$ may be resolved only if the noise level is less than 0.01%, i.e., $p < 10^{-4}$. With the increasing distance between local relaxation processes, the tolerable level of noise increases. For relaxation processes half a decade apart, the tolerable noise level is 0.1% and for relaxation processes one decade apart the noise level may be as high as 1%.

Even if all the above-mentioned corrections are implemented, the ratio E/S remains noisy and may be used for the inverse transformation only up to a certain value $i = i_{max}$. The selection of the suitable i_{max} still poses a difficulty and is to some extent arbitrary; however, there is a certain range of i where the values of the ratio E/S decrease to a negligible value, so that the choice of the truncation point i_{max} is not so critical. The

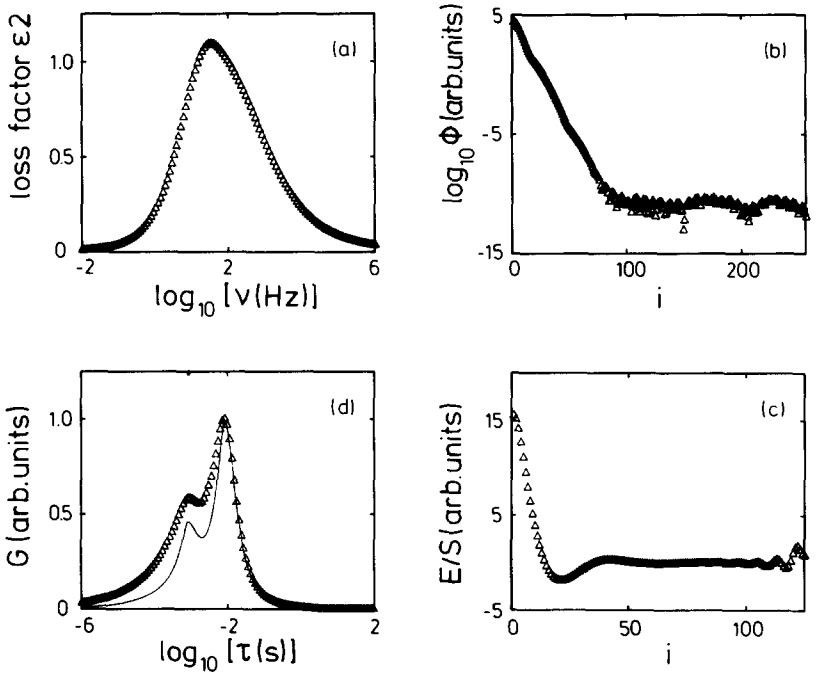

Fig. 4. (a) Loss factor vs. frequency generated from two Havriliak–Negami distributions (same as in fig. 1(c)). (b) Power spectral density vs. point number (proportional to relative frequency). (c) Ratio E/S (see text) vs. point numbers. (d) Distribution, $G(u)$, pertaining to loss factor in fig. 1(a). △ calculated values; ———, theoretical values.

truncation point may also be suggested from the changes of the behaviour of the curve in the $\Phi(f)$ plot, where the presence of noise and truncation effects is more pronounced than in the FT itself.

3. Test of the method

The applicability of the method was tested using both simulated as well as experimental data. Some typical results are reported.

In the first case, the calculation of $G(u)$ was carried out on the sum of two HN distributions with parameters $\alpha_1 = \alpha_2 = 0.2$, $\gamma_1 = 0.7$, $\gamma_2 = 0.5$, $\tau_1 = 0.01$ s, $\tau_2 = 0.001$ s, relative weights $\Delta\epsilon_1 = 3$, $\Delta\epsilon_2 = 1.5$ in the interval 10^{-2}–10^{6} Hz with 128 points. The simulated $\epsilon''(f)$ is shown in fig. 4(a). Apparently, the relaxations merge and cannot be distinguished. The $\epsilon''(f)$ curve was extrapolated to 512 points using eq. (31) and shifted in such a way that the border values of ϵ'' were equal. The corresponding PD $\Phi(f)$ is shown in fig. 4(b), and the ratio E/S in fig. 4(c). Both figs. 4(b) and (c) may be used to assess the truncation point. In fig. 4(b) the steep decrease of $\Phi(f)$ for $i < 100$ changes into an almost straight noisy line which is interpreted as the commencing dominance of $\Phi(f)$ by noise. Similarly, the ratio E/S decreases in the region $0 < 100$ to zero (non-monotonically), and then starts to oscillate with a large amplitude. Therefore, setting $i_{max} = 100$–120 seems to be a suitable choice. After truncating E/S at 110 points and inverting the result, $G(u)$ is obtained and shown in fig. 4(d). The choice of the truncation point is not critical – truncating the ratio E/S at 122 points results in a slightly more noisy $G(u)$ curve only. The positions of the local relaxation maxima are recovered, although the shape of calculated $G(u)$ departs slightly from the theoretical curve. It is important that no spurious peaks appear.

In the second example, a set of measured data was chosen. These are the measurements on a sample of poly-n-butyl-acrylate in the frequency range 300 Hz–6 MHz at 223.16 K. The input data of $\epsilon''(f)$ are shown in fig. 5(a). Only one relax-

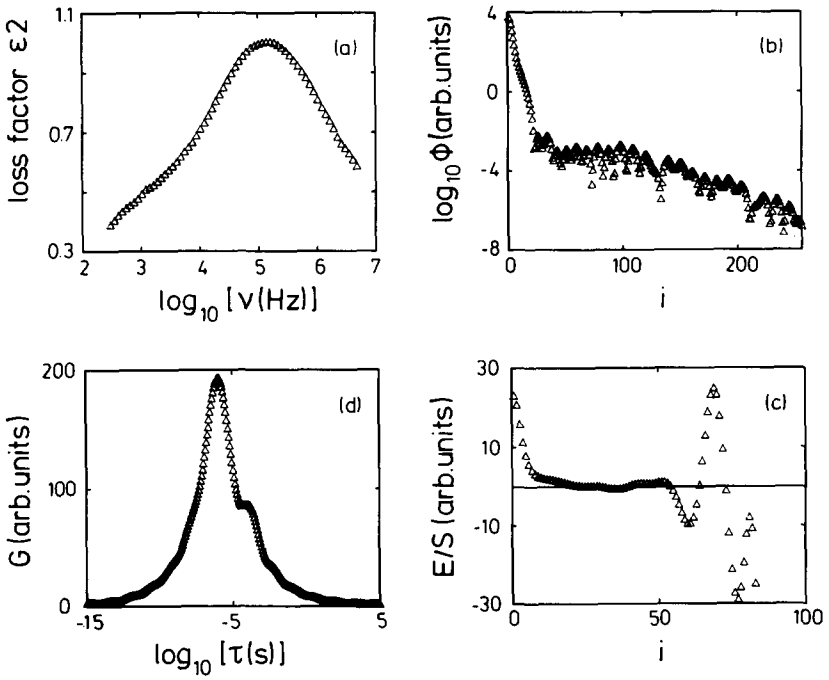

Fig. 5. (a) Loss factor vs. frequency of a sample of poly-n-butyl-acrylate at 229.3 K. (b) Power spectral density vs. point number. (c) Ratio E/S vs. point number. (d) Calculated distribution of relaxation times.

ation maximum is visible, but the change of slope of $\epsilon''(f)$ at low frequencies indicates a more complex relaxation structure. The determination of the position of the second relaxation mechanism by conventional methods (e.g., fitting) from the data in fig. 5(a) seems impossible. The data were again extrapolated according to eq. (31) and shifted as described above. Power spectral density (PSD) of the extrapolated loss factor is shown in fig. 5(b), and the ratio E/S in fig. 5(c). Again, as in the preceding case, both $\Phi(f)$ and E/S may be used to estimate the best suitable truncation point. For $40 < i < 60$, the steep decrease of PSD changes to a slow noisy decay marking the onset of noise. This onset is even more marked in fig. 5(c), where the oscillatory behaviour sets in at about $i \simeq 50$, so that a choice $i_{max} = 45$–55 seems reasonable. In view of the fact that the data are experimental, not simulated, the level of noise is higher than in the preceding case, thus yielding fewer points for the inverse FT. The shape of $G(u)$ is shown in fig. 5(d). Two relaxation mechanisms are clearly visible and the positions of the peaks can be determined. Again, no spurious peaks appear.

Figures 4(d) and 5(d) show at the same time the inherent limits of the method. The distribution of relaxation times, $G(u)$, is recovered only in numerical form as opposed to fitting which yields analytical formulas. Therefore local relaxation mechanisms may be resolved in $G(u)$ only as long as they are visible there.

4. Conclusion

Testing has proved that the deconvolution method may be practically applied to the analysis of complex relaxation phenomena in dielectrics. With the simulated data, the present method is able to discern relaxation maxima differing by a factor of two, provided they are still visible in the distribution $G(u)$.

The truncation of the ratio E/S remains a problem to be addressed. The correcting procedures available (extrapolation, Hanning window, polynomial interpolation, curve shifting and noise reduction) separate the noise from the 'true' FT of $G(u)$ more distinctly, so that the exact choice of the truncation point is not critical. However, the noise limits the recovery of $G(u)$ from the experimental data and because the further details of E/S are smeared in the noise, finer structure of $G(u)$ is lost.

In conclusion, it is necessary to emphasize that the deconvolution method just enables the mathematical solution of eq. (4) but it says nothing about the physical acceptability of the solution. Therefore, it cannot decide whether the observed $\epsilon''(f)$ is due to the distribution of relaxation times or to some other in itself non-exponential behaviour.

This work was carried out in the framework of the Sonderforschungsbereich 262. A scholarship from the Deutscher Akademischer Austauschdienst for K.L. is gratefully acknowledged. Samples were kindly provided by Dr A. Müller, Fachbereich Physikalische Chemie, Universität Mainz. Discussion with Dr F. Kremer, MPI-Polymerforschung is particularly appreciated.

References

[1] A.K. Rajagopal and K.L. Ngai, in: Relaxation in Complex Systems, eds. K.L. Ngai and G.B. Wright (Naval Research Lab., Washington, 1984) p. 275.
[2] L.A. Dissado and R.M. Hill, Solid State Ionics 22 (1987) 331.
[3] R.G. Palmer, D.L. Stein, E. Abrahams and P.W. Anderson, Phys. Rev. Lett. 53 (1984) 958.
[4] C.J.F. Böttcher and P. Bordewijk, Theory of Electric Polarization, 2nd Ed. (Elsevier, Amsterdam, 1978).
[5] K. Schmidt-Rohr and H.W. Spiess, Phys. Rev. Lett. 66 (1991) 3020.
[6] G.P. Johari, J. Chim. Phys. 82 (1985) 283.
[7] Lei Wu, Phys. Rev. B43 (1991) 9906.
[8] N.G. McCrum, B.E. Read and G. Williams, Anelastic and Dielectric Effects in Polymeric Solids (Wiley, New York, 1967).
[9] P. Colonomos and R.G. Gordon, J. Chem. Phys. 71 (1979) 1159.
[10] J.G. McWhirter and E.R. Pike, J. Phys. A11 (1978) 1729.
[11] Y. Imanishi, K. Adachi and T. Kotaka, J. Chem. Phys. 89 (1988) 7593.
[12] A.D. Franklin and H.J. de Bruin, Phys. Status Solidi (a)75 (1983) 647.

[13] D.L. Misell and R.J. Sheppard, J. Phys. D6 (1973) 379.
[14] W.H. Press, B.P. Flannery, S.A. Teukolsky and W.T. Vetterling, Numerical Recipes – The Art of Scientific Computing (Cambridge University, Cambridge, 1988).
[15] T.R. Clune, Intell. Instrum. Comp. 7 (1989) 103.
[16] E.O. Brigham, The Fast Fourier Transform (Prentice Hall, Englewood Cliffs, NJ, 1974).
[17] Y. Dutuit, Rev. Phys. Appl. 14 (1979) 939.
[18] A. Erdelyi, ed., Tables of Integral Transforms (McGraw-Hill, New York, 1954).
[19] S. Sorella and S.K. Ghosh, Rev. Sci. Instrum. 55 (1984) 1348.
[20] L.R. Rabiner and B. Gold, Theory and Application of Digital Signal Processing (Prentice Hall, Englewood Cliffs, NJ, 1976).
[21] M. Froeyen and L. Hellemans, Rev. Sci. Instrum. 56 (1985) 2325.